Journal of The Electrochemical Society, 2020 **167** 062509

Ruthenium Electrodeposition from Water-in-Salt Electrolytes and the Influence of Tetrabutylammonium

William D. Sides* and **Qiang Huang***,z

Department of Chemical and Biological Engineering, University of Alabama, Tuscaloosa 35487, United States of America

The use of water-in-salt electrolytes is evaluated for the electrodeposition of metallic ruthenium. The mechanisms of proton reduction inhibition by concentrated LiCl and dilute tetrabutylammonium is evaluated. Concentrated LiCl is found to disrupt the hydrogen bonding network within the solution bulk, whereas TBA is found to adsorb onto the electrode surface, blocking proton access. Ruthenium exists as a different complexed species in water-in-salt electrolytes vs dilute aqueous electrolytes, leading to a −300 mV shift in the deposition onset potential. Greater current efficiencies of Ru deposition can be obtained when depositing at proton overpotentials by the use of water-in-salt electrolytes, and TBA can offer further improvements. The grain structure and resistivities of Ru thin films are studied.

© 2020 The Author(s). Published on behalf of The Electrochemical Society by IOP Publishing Limited. This is an open access article distributed under the terms of the Creative Commons Attribution Non-Commercial No Derivatives 4.0 License (CC BY-NC-ND, http://creativecommons.org/licenses/by-nc-nd/4.0/), which permits non-commercial reuse, distribution, and reproduction in any medium, provided the original work is not changed in any way and is properly cited. For permission for commercial reuse, please email: oa@electrochem.org. [DOI: 10.1149/1945-7111/ab847e]

Manuscript submitted February 21, 2020; revised manuscript received March 19, 2020. Published April 14, 2020.

Supplementary material for this article is available online

As microchip interconnect dimensions continue to scale down, the use of electroplated copper as the interconnect material faces challenges due to its exponentially increasing resistance as trench dimensions narrow. This limitation has resulted in a need to develop damascene processes suitable for metallization with alternate metals that perform better in small trench dimensions. Ruthenium has been identified as a promising candidate to fill this need.[1–3] Its shorter electron inelastic mean free path vs copper indicates it will not be as susceptible to resistance increases as dimensions narrow.[4,5] Additionally, Ru has been shown to have superior robustness against both oxidation and electromigration, one of the primary modes of interconnect failure.[6] Perhaps equally as importantly, Ru is stable when in direct contact with dielectric surrounding the trench, eliminating the need for a diffusion barrier typically implemented in copper interconnects. Barrierless Ru interconnects allow the entire cross section of the trench to be occupied by conductor, providing a much more efficient use of space, particularly as trench widths come well within the same order of magnitude of the typical diffusion barrier thickness.[3] Recently, explorations into the use of ruthenium for interconnect applications have primarily employed chemical vapor deposition methods.[6] While results have indeed demonstrated excellent potential, the use of CVD presents challenges in terms of achievable film purity and growth rates.

A Ru electrodeposition process analogous to the ubiquitous process for copper damascene metallization would certainly be a significant achievement toward enabling the deployment of Ru based interconnect technology. Electrochemical deposition of Ru metal has proven challenging, owing to its tendency to form oxides.[7–11] The formation of metallic Ru deposits requires electrodeposition at potentials negative with respect to the proton reduction potential.[12,13] The resulting low current efficiency inevitably causes hydrogen embrittlement and can cause cracking to occur in films. Commercial Ru electroplating methods also call for bath temperatures to be elevated to up to 80 °C to improve current efficiencies[14]—a condition that would impose challenges for wafer processing tools such as vapor evaporation and bath control, stability of anolyte membranes, humidity control in the tool chamber, and oxide control on wafers.

Water-in-salt electrolytes (WiSE) have recently emerged as a promising tool to decrease the amount of hydrogen evolved during metal electrodeposition at overpotentials to proton reduction.[15–17] Recently receiving significant attention from the lithium ion battery field as a solvent to enable high voltage aqueous batteries, WiSE contain extremely high concentrations of salt, such as LiCl.[18–21] The concentration of salt is high enough that every water molecule is contained within the primary solvation sheath of a solute ion, hence the name water-in-salt. The use of WiSE allows the formation of a mass transport limiting current of the hydrogen evolution reaction (HER) in a very acidic electrolyte, which enables metal deposition at potentials significantly negative to the onset of HER while maintaining reasonable current efficiencies. Our group has shown that this is due to a significant decrease of the proton diffusion coefficient in WiSE.[15] Concentrated alkaline metal cations disrupt the extensive hydrogen bond network, hindering the so-called Grotthuss mechanism and significantly slowing proton diffusion.[22] Here, we describe efforts to implement a WiSE for the electrodeposition of ruthenium. The electrochemical behavior of the system is studied, and electroplated Ru films are characterized with an emphasis on crystal structure and resistivity of the deposited films. In addition, the effect of the hydrophobic tetrabutylammonium (TBA) cation on ruthenium deposition is studied and efforts are devoted to elucidating the mechanism of suppression.

Methods

All electrolytes were made up of 18.2 MΩ · cm water and 0.1 M ACS grade H_2SO_4. WiSE also contained 5 M LiCl (98%) and certain solutions contained various amounts of tetrabutylammonium hydrogen sulfate (98%). Electrolytes for metal deposition contained 25 mM hydrated $RuCl_3$. All electrochemical work was performed in a 3-compartment cell consisting of a platinum foil counter electrode separated from the cathode by a glass frit and a saturated calomel reference electrode (SCE) fixed in position through a Luggin capillary. All potentials reported in this work are with respect to the SCE. The total solution volume within the cell was 100 ml. CV studies and potentiostatic depositions for partial current and current efficiency measurements were performed on a 5 mm diameter Pt rotating disk electrode (RDE). Voltammetric sweeps were performed at 100 mV s^{-1}, which is sufficiently fast to complete experiments before significant buildup of hydrogen bubbles can occur on the electrode surface. Ruthenium partial currents and efficiencies were measured by electroplating Ru for 60 s at 400 RPM, followed immediately by rinsing with DI water and immersion into a 0.1 M KOH solution at an applied potential of 0.45 V. The integrated stripping charge was used to calculate the amount of Ru deposited using Faraday's law, assuming the Ru cathodically deposits with a 3-

*Electrochemical Society Member.
zE-mail: qhuang@eng.ua.edu

electron reduction, and anodically strips with a 7-electron oxidation, as indicated by the Pourbaix diagram.[23] The detailed stripping curves of typical electrodeposited Ru films are shown in Fig. S-1 in the Supplementary Information (available online at stacks.iop.org/JES/167/062509/mmedia). The anodic stripping current peak of a thin Ru film could be well resolved from oxygen evolution reaction (OER) by the LSV condition used. The OER rate is negligible compared with Ru stripping at a constant potential of 0.45 V, and an endpoint of the stripping can be easily determined and stripping charge easily obtained. Furthermore, this method was verified by comparing the ruthenium deposit mass calculated by this stripping method to the deposit mass determined through X-ray fluorescence (XRF) analysis during a set of preliminary experiments in this system, as shown in Fig. S-1 in the Supplementary Information. Potentiostatic deposition experiments with the injection of TBA were carried out on a stationary Pt electrode prepared by masking Pt foil with platers tape, exposing a 6 mm diameter circular Pt surface. This was mounted into the cell vertically and vigorous N_2 bubbling within the cathode compartment provided agitation and rapid removal of H_2 bubbles from the electrode surface. A solution of 100 mM TBA was injected into the cell in the appropriate amounts.

Thin film Ru samples were deposited on silicon coupons with Pd strips as seed layers. These substrates were prepared by first thermally depositing a 50 nm layer of SiO_2 onto a Si wafer. The wafer was then patterned using lithography to create a 1 mm by 10 mm strip connected to a 3 mm by 5 mm contact pad. A 10 nm layer of Ti followed by a 110 nm layer of Pd was evaporated. The photoresist was lifted off, leaving the patterned substrates. These substrates were mounted onto a chuck rotating in the same way as the RDE. Electrical connection was made through a front contact pin to the pad. The Pd seed resistance was measured directly and the resistivity was calculated as $1.46 \pm 0.04 \times 10^{-7}\ \Omega$ m.

Raman spectroscopy was performed on a Horiba LabRAM HR with a 532 nm laser. An Autolab 302 N potentiostat with a frequency analyzer was used for all electrochemical work. Solution resistance was determined through electrochemical impedance spectroscopy, wherein a sinusoidal potential was applied with an RMS amplitude of 10 mV and the frequency was sampled from 0.1 Hz to 100 kHz. The solution resistance was used to correct for ohmic voltage drop in results where indicated. Thin film strip samples were cleaved from the contact pad after deposition. Film thickness was measured using a KLA Alpha-Step D-500 stylus profilometer. Measurements spanned the entire width of the strip length and were averaged over at least 3 points in the central third of the strip length. Resistances were measured using a linear four-point probe that spanned 6 mm along the centerline of the strip. The spacing between the probes was 2 mm, and the strip width was 1 mm, so a uniform current distribution was assumed, and no shape correction factors were used. X-ray diffraction (XRD) measurements were performed on a Bruker D8 Discover with GADDS and a Co Kα X-ray source (wavelength = 1.79 Å). Annealing was performed in a home-built vacuum furnace using ultra high purity helium as the purging gas and an operation pressure below 1E-5 Torr.

Results and Discussion

Tetrabutylammonium additive and water-in-salt electrolyte.— Recently published work from our groups has thoroughly investigated the mechanism of HER suppression by concentrated LiCl, and

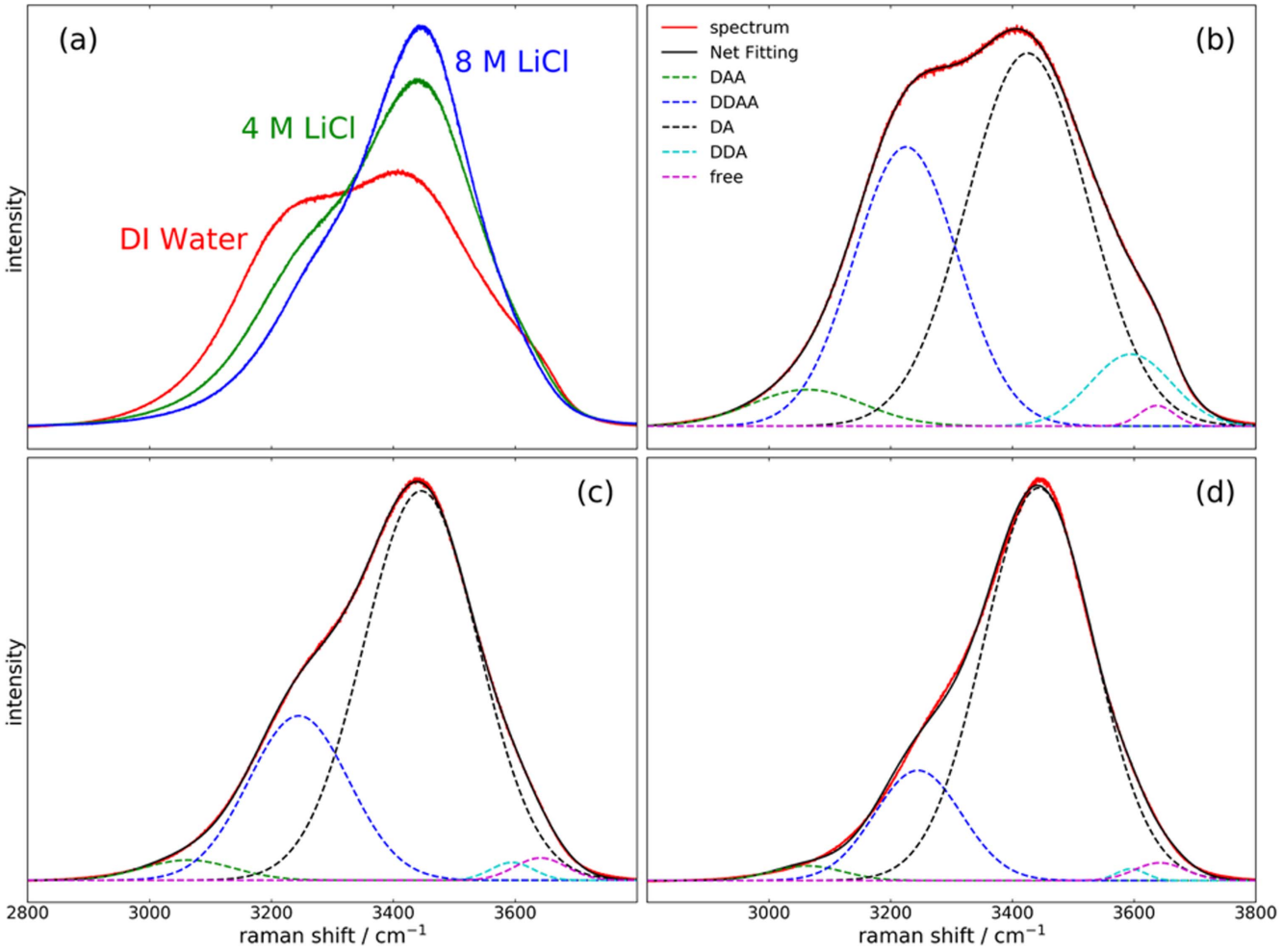

Figure 1. (a) Raman spectra of water with various amounts of LiCl, and deconvolutions of the peaks for (b) DI Water, (c) 4 M LiCl, and (d) 8 M LiCl.

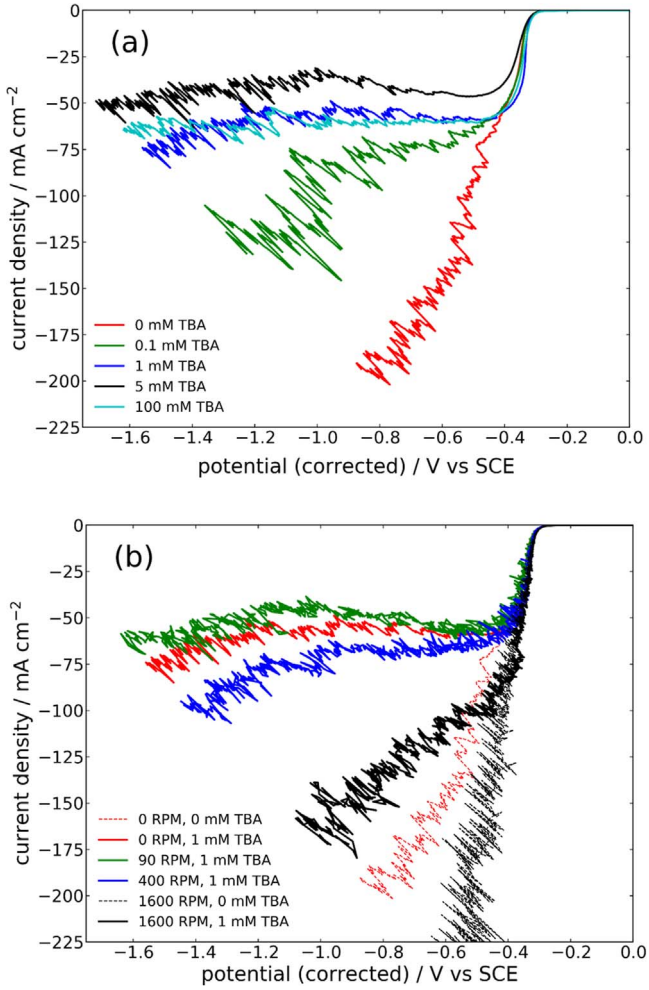

Figure 2. CVs of 0.1 M H_2SO_4 with (a) various concentrations of TBA in quiescent conditions, and (b) with and without 1 mM TBA at various rotation rates.

concluded that it is primarily due to an order-of-magnitude decrease in the proton diffusion coefficient arising from a disruption of the extensive hydrogen bond network within water, primarily attributable to the alkali metal cation.[15] No significant change is imparted on the diffusion coefficient of metal cations by the introduction of LiCl. The hydrogen bonding state of water molecules in solution can be conveniently observed by Raman spectroscopy.[24–27] The OH stretch band of water molecules gives rise to a broad peak at around 3400 cm^{-1}. Although there is some controversy over the exact nature of this peak,[28] it is generally understood that it can be deconvoluted into 5 gaussian peaks corresponding to the primary hydrogen bonding states of water molecules. These hydrogen bonding states include DAA (single donor, dual acceptor), DDAA (dual donor, dual acceptor), DA (single donor, single acceptor), DDA (dual donor, single acceptor), and free (non-hydrogen bonding) molecules, and are centered respectively at 3063 cm^{-1}, 3225 cm^{-1}, 3424 cm^{-1}, 3595 cm^{-1}, and 3637 cm^{-1} based on fitting of our measured spectra and in close agreement with literature. By comparing the size of these fitted peaks, it is simple to examine differences in the hydrogen bond network under different conditions. Figure 1a shows the Raman spectrum of DI water under ambient conditions, as well as spectra of a 4 M and an 8 M LiCl solution. Significant changes of the OH stretch band are observed. Deconvolution of the peaks, shown in Figs. 1b–1d, reveals a significant shift away from the DAA, DDA, and tetrahedrally bonded DDAA states and toward the DA state as the LiCl concentration is increased to 8 M. This shift away from higher bonding states toward lower bonding states confirms that concentrated LiCl significantly disrupts the hydrogen bonding network, preventing fast proton diffusivity via the Grotthuss mechanism.

Proton reduction kinetics can be further suppressed by the addition of TBA to plating baths. This hydrophobic cation has been shown to block water molecules from accessing the cathode surface in organic solvents, preventing water reduction.[29] We have recently reported the ability of TBA to suppress HER during metal deposition at potentials more negative than proton reduction, in both WiSE and conventional dilute electrolytes.[30] Detailed studies are carried out here to probe the mechanism of this observation. Stationary CVs in 0.1 M H_2SO_4 have been performed to study the effects of additions of TBA on proton reduction. The cathodic linear sweep voltammograms (LSVs) are shown in Fig. 2a. In all cases, noise in the data is attributed to hydrogen bubbles, which first block and then detached from the electrode resulting changes in the electrode surface area. The prevailing "slope" observed in the noise is a result of the post-experiment IR correction. Without TBA, proton reduction onsets at −0.25 V and the rate exponentially increases without mass transport limitations as the applied potential is swept to −2 V. When corrected for solution IR drop, the electrode potential is limited to −0.8 V. The addition of 0.1 to 100 mM TBA to the electrolyte is seen to inhibit the proton reduction, with significant inhibition occurring at the smallest tested concentration of 0.1 mM and the effect becoming saturated at 1 mM TBA. Significantly more negative electrode potentials beyond −1.6 V become achievable at the same applied potential of −2 V. The small additions of TBA are not expected to significantly change the solution resistance, rather a more negative electrode potential is possible due to a much lower proton reduction current and thus a much smaller IR drop. The current density becomes limited to less than 75 mA cm^{-2} throughout this range. A proton mass transport limiting current is not expected to manifest here, particularly as the dilute nature of the additive should not have a significant effect on the proton diffusivity. Instead, an interface phenomenon such as surface adsorbed TBA cations hindering the charge transfer or blocking proton adsorption likely gives rise to this current limitation. Inspection of the potential region positive of −0.4 V shows that TBA does not generally result in negative current deviations from the additive-free electrolyte until more cathodic potentials are reached, and deviations become greater at more negative potentials. This suggests a potential-dependent adsorption process, where TBA absorbs on the electrode surface to a greater extent at more negative potentials. An alternative explanation could involve a TBA–OH precipitate forming and blocking the electrode surface at the high surface pH conditions that are generated at highly negative potentials, however this possibility can be discounted on the basis of the pre-derivatization studies discussed below. Therefore, at highly negative potentials, TBA competes with hydrogen atoms for adsorption sites, preventing the adsorption of hydrogen atoms necessary for hydrogen evolution through the Volmer-Heyrovsky mechanism. While adsorbed TBA has been previously reported to prevent water reduction due to its hydrophobicity blocking access to the cathode, here it is suspected that a similar blocking of hydronium ions can inhibit proton reduction. Again, the effect of TBA here seems to saturate at 1 ppm and the small differences between the currents at 1, 5, and 100 ppm TBA are likely due to experimental errors.

The HER suppressing effects of 1 mM TBA has been studied under rotating conditions as shown in Fig. 2b. Gentle rotation up to 90 RPM has little effect on the suppression of proton reduction, however rotation of 400 RPM results in a slight increase of the proton reduction rate and rotating at 1600 RPM results in a proton reduction current with much less deviation from the additive-free case. While we believe that TBA adsorbs on the electrode surface by a potential dependent mechanism, another possibility is that insoluble TBA hydroxides are formed at the electrode surface. As the potential becomes more negative, the hydroxide concentration near the electrode surface increases due to proton and water reduction,

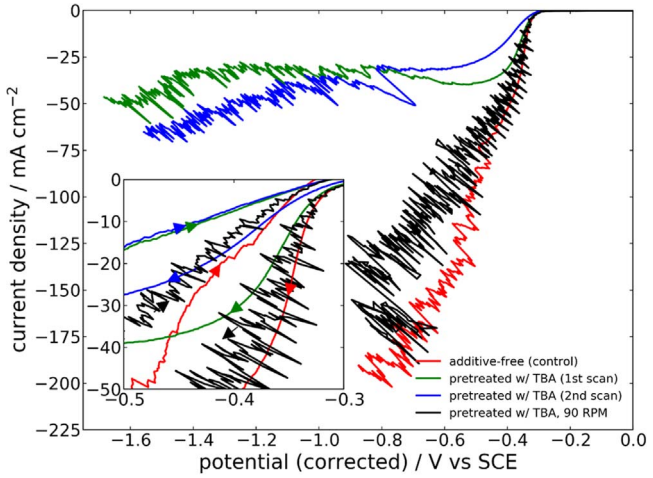

Figure 3. Cathodic direction sweeps of CVs on an electrode pre-derivatized with TBA in 0.1 M H_2SO_4. Two cycles are shown on a stationary electrode, with a potential of +1.5 V reached in the anodic direction between the scans. One cycle is shown on an pre-derivatized electrode rotating at 90 RPM. Inset shows full CV (both cathodic and anodic direction sweeps).

resulting in a potential dependent formation of the insoluble TBA hydroxides. The less suppression observed at a higher rotation rate seems to be consistent with this alternative explanation as well, because a higher rotation rate mitigates the depletion of proton or pH increases at the surface. To determine whether this is the cause of proton reduction suppression, CVs were performed in additive-free electrolyte on an electrode surface that had been derivatized with TBA by immersion in 100 mM TBA for 5 min at open circuit, followed by brief, gentle immersion in DI water to remove excess TBA, and gentle immersion into the additive-free electrolyte. Two CV cycles were performed, beginning at 0 V and sweeping in a negative direction, with an anodic vertex of 1.5 V reached between the two scans, shown in Fig. 3. The suppressing effect on proton reduction is clearly observed on this derivatized electrode with no TBA in the electrolyte bulk, proving that this suppression is an interface effect. No further TBA adsorption can occur during this CV, so no potential dependent adsorption process is expected in this experiment, and the inset in Fig. 3 shows clearly that proton reduction is inhibited from the onset. The second consecutive cycle in the CV shows similar inhibition, despite the fact that the electrode had been swept to a positive potential (+1.5 V) that might be expected to accelerate the desorption of cationic TBA. Anodic vertices up to +2.0 V were tested (not shown) and did not result in any apparent desorption of TBA. That the inhibiting effect remains nearly identical on the second scan suggests that TBA desorption is either not induced by positive polarization of the electrode or that it has slow kinetics. Gentle rotation (90 RPM) of a TBA derivatized electrode during a CV scan in additive-free electrolyte eliminates any HER inhibiting effect, indicating that electrolyte flow over the electrode surface is sufficient to cause desorption of TBA. It seems unusual that TBA adsorption is strong enough to prevent desorption even after a period of 30 s including a rinse in DI water, yet TBA is flushed off seemingly immediately by 90 RPM rotation during the CV scan. This observation is consistent with the absence of suppression at high rotation rates, particularly 1600 rpm, seen in Fig. 1b. The nature and strength of TBA adsorption warrant further examination. Nonetheless, the fact that suppression can be observed with only the TBA surface layer without TBA in the bulk solution indicates that the suppression is not due to the formation of an insoluble TBA hydroxide blocking layer.

The dependence of proton reduction suppression on TBA concentration was examined with a chronoamperometry experiment shown in Fig. 4. A Pt foil electrode was mounted vertically in the additive-free electrolyte to allow easy escape of H_2 bubbles, agitation was provided by vigorous N_2 gas bubbling, and the applied potential was held at −1.5 V while current was recorded. Despite an experimental setup designed to aid the rapid removal of hydrogen bubbles, their generation at the electrode resulted in quite a bit of noise in the data, so cyan colored lines are plotted in Fig. 4 at the mean current value for each injection period. TBA was injected at the indicated times, and it was found that 50 μM of TBA in solution was sufficient to achieve a noticeable decrease in HER current of 20%. Once a total of 500 μM of TBA had been injected into solution, a 56% decrease in HER current was achieved, and further additions of TBA did not further decrease the HER current.

The proton reduction inhibition at the interface by TBA was found to compound with the decrease of proton diffusivity in the bulk electrolyte caused by concentrated LiCl. Figure 5 shows a CV on a Pt electrode in 0.1 M H_2SO_4, and the individual and combined effects of 1 mM TBA and 5 M LiCl. It is notable that while water reduction is almost entirely inhibited in the case of TBA only, electrolytes containing LiCl see an onset of significant water reduction at −1.0 to −1.2 V, consistent with the increased Lewis acidity of water molecules coordinated with Li cations in the bulk of the solution.[15] Despite this, there is a potential window from the proton reduction onset until about −1.1 V where the combined effects of TBA and LiCl limit the current of the HER to below 20 mA cm^{-2}. Electrode potentials even more negative than this are achievable, albeit with an increasing rate of hydrogen evolution. Such an expanded electrochemical window in acid aqueous solutions promises to enable the electrodeposition of less noble metals or metal ion complexes from aqueous solutions.

Ruthenium deposition.—The electrodeposition of Ru was studied from WiSE and the effects of TBA additive were examined. Plating baths were made by dissolving hydrated ruthenium trichloride into the electrolyte to be studied, followed by the addition of TBA if desired. A 3-electron reduction from Ru(III) to Ru metal is assumed for partial current and current efficiency calculations, despite the fact that the plating bath can be expected to contain some amount of Ru(IV) species.[14,31,32] The coordination chemistry of ruthenium chloride solutions is complex,[33] and the exact nature of the ruthenium species involved is outside the scope of this work. It will be referred to here as Ru(III) rather than Ru^{3+} to reflect its oxidation valence. It was observed that dissolving both the black ruthenium salt and 5 M LiCl into the same solution was accompanied by gas bubble formation within the solution and a change in solution color from black to red, seen in Fig. 6, indicative of a change in the dominant Ru species. No attempt was made to identify the evolved gas. The dissolution of LiCl in water is exothermic. While the solution did not get hot enough to support water boiling, a lower solubility of air at an elevated temperature may have contributed to the formation of such bubbles, despite of an increased amount when $RuCl_3$ and LiCl are dissolved simultaneously. Dissolution of the ruthenium salt in a LiCl-free electrolyte did not result in color change or gas formation.

Electrodeposition of Ru is accompanied by significant hydrogen evolution resulting in a low current efficiency. Figure 7 shows partial current densities of ruthenium deposition and current efficiencies in both additive-free electrolytes and ones containing 5 M LiCl and/or 1 mM TBA. A rotation rate of 400 RPM was used to prevent accumulation of H_2 bubbles on the electrode surface. In the LiCl-free electrolytes, Ru deposition has an onset potential of −0.2 V, at nearly the same position as the onset of proton reduction. As the complexation of the Ru species are not known, direct comparisons to reduction potentials found in the literature cannot be made. A shift of approximately −300 mV in the onset potential of Ru deposition is noticed when depositing from LiCl containing electrolyte, likely caused by differing Ru complexation chemistry between the two electrolytes. The use of 5 M LiCl, however, allows a greater Ru deposition rate to be obtained with a maximum of −4.3 mA cm^{-2} at an electrode potential of −0.8 V. As observed for other metal depositions,[15,17] the presence of concentrated LiCl in the plating

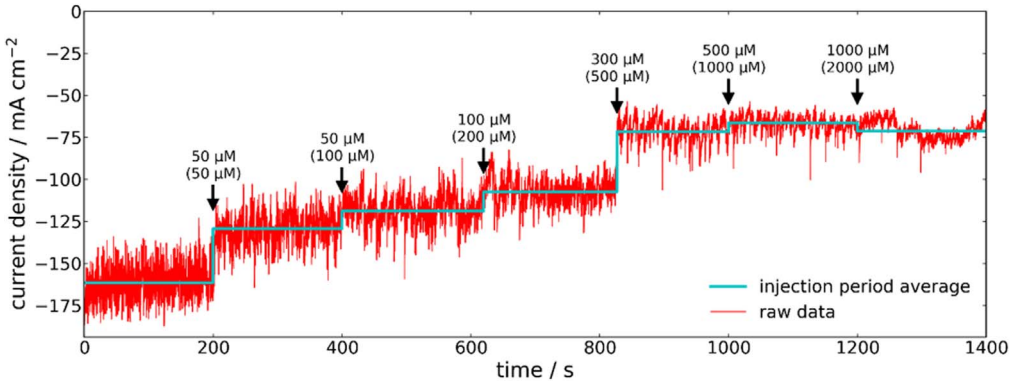

Figure 4. Current on a stationary Pt electrode during a potentiostatic hold at −1.5 V (applied) in 0.1 M H_2SO_4 during TBA injections of the indicated amount (total amount). Agitation provided by rigorous N_2 bubbling. The average current during each injection period is shown by the cyan line.

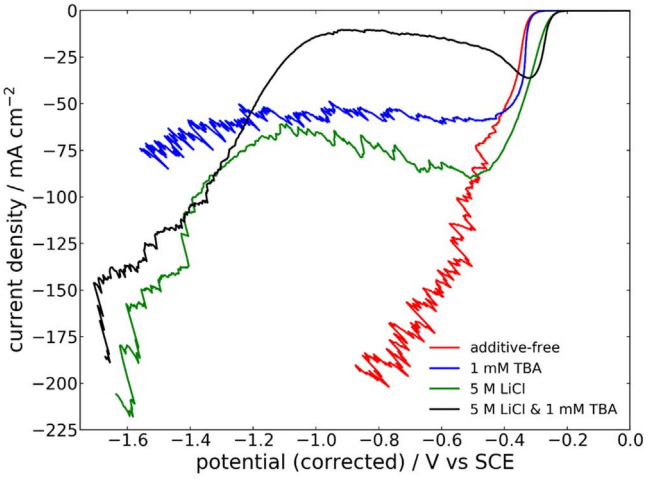

Figure 5. CVs of a Pt electrode in quiescent conditions in 0.1 M H_2SO_4 with and without 1 mM TBA and/or 5 M LiCl.

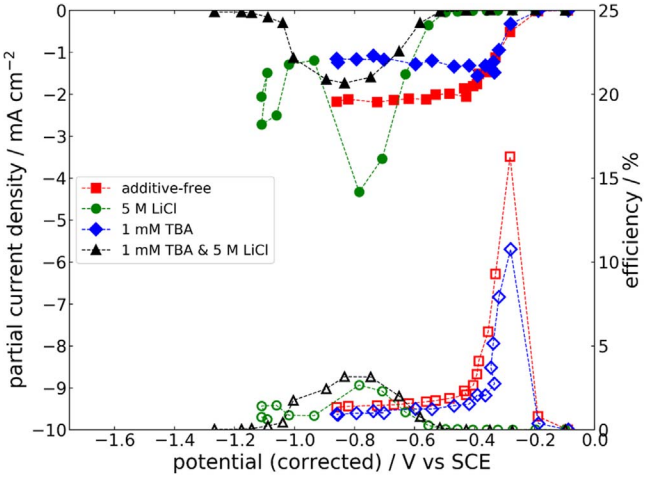

Figure 7. Ruthenium deposition partial currents (solid markers) and current efficiencies (outlined markers) in various electrolytes at 400 RPM.

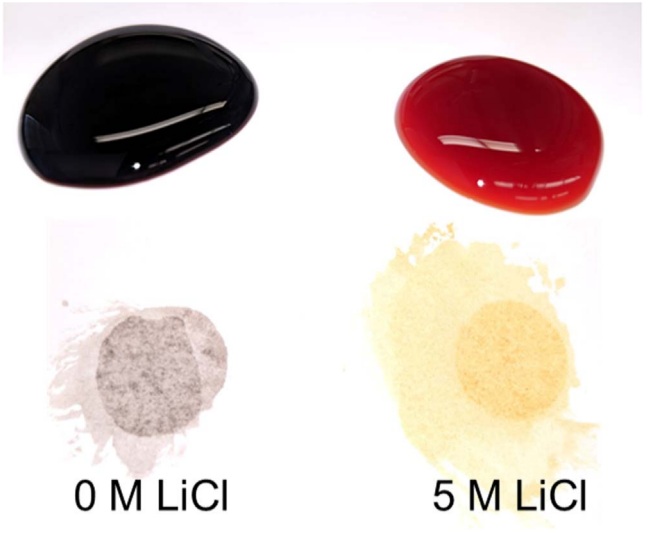

Figure 6. Photographs of Ru solutions as drops and paper stains.

bath resulted in a decrease in Ru deposition partial current at highly cathodic potentials. Although the potential at which this occurs for Ru deposition is slightly obscured by experimental noise (likely due to hydrogen bubble blockage of the electrode surface) in the TBA free electrolyte, this effect is clearly observed here in the TBA containing electrolyte. This can be attributed to the formation of a poorly soluble hydroxide species at the electrode that blocks subsequent metal deposition. This could be either LiOH or ruthenium hydroxide that forms in the presence of OH^- liberated from water at highly cathodic electrode potentials. Potentials more negative than −0.9 V were not achieved in LiCl free electrolyte, so it is unknown if a similar effect would occur at these negative potentials in dilute electrolytes.

The addition of TBA suppresses the deposition of Ru in the dilute aqueous electrolyte, limiting the partial current to $-1.2\ mA\ cm^{-2}$ as opposed to the limiting current of $-2.2\ mA\ cm^{-2}$ that is attained from additive-free electrolyte. A similar suppression is observed in solutions containing 5 M LiCl upon addition of TBA. Although it is apparent that adsorbed TBA inhibits both Ru deposition and proton reduction, the inhibiting effect on proton reduction is greater than that on Ru deposition, leading to a 20% increase in peak current efficiency when TBA is used in a 5 M LiCl solution. A greater increase in current efficiency is expected if the rotation rate is reduced to 90 RPM or below, owing to a greater effectiveness of TBA. However, taking similar partial current measurements at lower rotation rates becomes more challenging as H_2 bubbles accumulate on the electrode surface, particularly in less-suppressed electrolytes. The use of 5 M LiCl, particularly when combined with TBA, allows for Ru electrodeposition at improved current efficiencies between about −0.6 V and the onset of water reduction. While current efficiencies are highest in the potential range from −0.2 to −0.4 V in LiCl free electrolytes, plating rates in this region are low, with the greatest current efficiency at a Ru partial current of only $-0.52\ mA\ cm^{-2}$. Additionally, the ability to operate at highly

negative potentials provides the flexibility to perform alloy electroplating with less noble metals.

Four Ru thin film samples have been electrodeposited from an additive free electrolyte and six from an electrolyte containing 5 M LiCl to study the differences in some properties relevant to interconnect applications, including resistivity and crystallinity. Depositions were performed at −0.5 V (corrected) and −1.0 V (corrected) in additive free and WiSE systems, respectively, with deposition times ranging from 5 to 20 min. Resulting film thicknesses cover a range from 215 nm to 1075 nm, thus a deposition rate at around 50 nm per minute. No thickness dependence was observed among the studied properties. Resistivities were calculated from the overall strip resistance using a model consisting of the Pd seed layer in parallel with the electrodeposited Ru thin film. The samples deposited from the additive-free electrolyte had resistivities of $1.09 \pm 0.2 \times 10^{-6}\,\Omega\,m$, whereas the samples deposited from the 5 M LiCl electrolyte has resistivities of $1.51 \pm 0.21 \times 10^{-6}\,\Omega\,m$. These values are significantly higher than reported bulk resistivity of Ru of $7.1 \times 10^{-8}\,\Omega\,m$,[34] a difference possibly accounted for by a high incorporation of chloride or other impurities within the deposit, and the nano-crystalline atomic order within the as-deposited films. X-ray diffractograms of as-deposited thin films presented in Fig. 8 have only very broad peaks corresponding to Ru crystal lattice, indicating that large grains are not formed. The morphology of a typical Ru films is shown as two top down scanning electron microscopy images in Fig. S-3 in Supplemental Information. The film was deposited at −1.0 V from an electrolyte containing 5 M LiCl, resulting in a smooth shiny film with nodules of sizes from 100 to 300 nm. However, such nodules are not single crystalline grains as depicted in XRD. Upon annealing for 60 min at 400 °C, an emergence of the Ru peaks is noted in samples deposited from solutions containing both 0 and 5 M LiCl, indicating that electrodeposited Ru can undergo grain growth at 400 °C despite the probable presence of impurities within the film. Despite grain growth upon annealing, no decrease in the resistivities could be measured. Delamination of the Ru thin film occurred near the edges of the strip during annealing, resulting in an irregular Ru strip and inaccurate resistivity calculation. A high incorporation of chloride was reported for rhenium deposition from this WiSE system.[30] Similarly high chloride incorporation in these Ru deposits are expected and are belived to contribute to an increase in resistivity.

Conclusions

The proton diffusivity decrease by concentrated LiCl is confirmed to be due to a disruption of the extensive hydrogen bonding network present within dilute solutions. The hydrophobic cation TBA adsorbs onto the electrode surface with a potential-dependent rate. While the resulted adsorbate is found to withstand gentle water rinse and even anodic biases, it breaks down upon a continuous strong agitation in a TBA free electrolyte. Upon adsorption, hydronium access to the surface is blocked and proton reduction to hydrogen is inhibited. The inhibiting effects of WiSE and TBA can be combined to significantly decrease the rate of hydrogen evolution, and provide an expanded electrochemical window beyond −1 V vs SCE, within which electrodeposition of materials can be feasibly performed. This has been proven for the electrodeposition of Ru, where, despite the transition to a less noble Ru complex found in water-in-salt electrolytes, Ru deposition can proceed with greater efficiency at potentials much more negative than proton reduction. Electrodeposited thin films were found to be nano-crystalline, however grain growth could be induced by annealing at 400 °C. Resistivities of the Ru films were higher than expected for bulk Ru, likely due to the nanocrystalline structure and impurities within the film.

Acknowledgments

The work is partially supported by National Science Foundation through a grant CMMI-1662332. The authors wish to thank Matthew Confer and Jair Lizarazo–Adarme for training and support on Raman and profilometer instrumentation, Rick Smith for making the electrochemical cells, and the University of Alabama Central Analytical Facility for support with XRD.

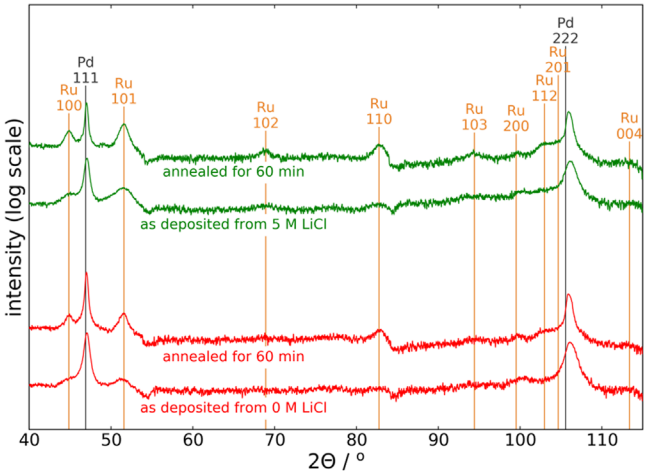

Figure 8. X-ray diffractograms of Ru thin films as-deposited from electrolytes containing 0 or 5 M LiCl, before and after annealing at 400 °C for 60 min.

ORCID

William D. Sides https://orcid.org/0000-0002-5884-4885
Qiang Huang https://orcid.org/0000-0002-1391-6531

References

1. C. Adelmann et al., "Alternative Metals for Advanced Interconnects."*2014 IEEE International Interconnect Technology Conference (IITC)*173 (2014).
2. D. Gall, "Electron mean free path in elemental metals." *J. Appl. Phys.*, **119**, 085101 (2016).
3. M. H. V. D. Veen et al., "Damascene benchmark of Ru, Co and Cu in scaled dimensions." *2018 IEEE International Interconnect Technology Conference (IITC)*, p. 172 (2018).
4. K. Fuchs, "The conductivity of thin metallic films according to the electron theory of metals." *Math. Proc. Cambridge Philos. Soc.*, **34**, 100 (1938).
5. E. H. Sondheimer, "The mean free path of electrons in metals." *Adv. Phys.*, **1**, 1 (1952).
6. Z. Xunyuan et al., "Ruthenium interconnect resistivity and reliability at 48 Nm Pitch." *2016 IEEE International Interconnect Technology Conference/Advanced Metallization Conference (IITC/AMC)*, p. 31 (2016).
7. C.-C. Hu, H.-R. Chiang, and C.-C. Wang, "Electrochemical and structural investigations of oxide films anodically formed on ruthenium-plated titanium electrodes in sulfuric acid." *J. Solid State Electrochem.*, **7**, 477 (2003).
8. I. Zhitomirsky and L. Gal-Or, "Ruthenium oxide deposits prepared by cathodic electrosynthesis." *Mater. Lett.*, **31**, 155 (1997).
9. F. Vigier, F. Gloaguen, J. M. Léger, and C. Lamy, "Electrochemical and spontaneous deposition of ruthenium at platinum electrodes for methanol oxidation: an electrochemical quartz crystal microbalance study." *Electrochim. Acta*, **46**, 4331 (2001).
10. C. C. Hu and Y. H. Huang, "Cyclic voltammetric deposition of hydrous ruthenium oxide for electrochemical capacitors." *J. Electrochem. Soc.*, **146**, 2465 (1999).
11. J.-J. Jow, H.-J. Lee, H.-R. Chen, M.-S. Wu, and T.-Y. Wei, "Anodic, cathodic and cyclic voltammetric deposition of ruthenium oxides from aqueous Rucl3 Solutions." *Electrochim. Acta*, **52**, 2625 (2007).
12. C. R. K. Rao and D. C. Trivedi, "Chemical and electrochemical depositions of platinum group metals and their applications." *Coord. Chem. Rev.*, **249**, 613 (2005).
13. D. K. Oppedisano, L. A. Jones, T. Junk, and S. K. Bhargava, "Ruthenium electrodeposition from aqueous solution at high cathodic overpotential." *J. Electrochem. Soc.*, **161**, D489 (2014).
14. T. Jones, "Electroplating of ruthenium." *Met. Finish.*, **6**, 121 (2001).
15. S. De, J. White, T. Brusuelas, C. Patton, A. Koh, and Q. Huang, "Electrochemical behavior of protons and cupric ions in water in salt electrolytes with alkaline metal chloride." *Electrochimica Acta*, **338**135852 (2020).
16. Q. Huang and Y. Hu, "Electrodeposition of superconducting rhenium with Water-in-Salt electrolyte." *J. Electrochem. Soc.*, **165**, D796 (2018).
17. Q. Huang and T. W. Lyons, "Electrodeposition of rhenium with suppressed hydrogen evolution from Water-in-Salt electrolyte." *Electrochem. Commun.*, **93**, 53 (2018).

18. L. Suo, Y.-S. Hu, H. Li, M. Armand, and L. Chen, "A new class of Solvent-in-Salt electrolyte for high-energy rechargeable metallic lithium batteries." *Nat. Commun.*, **4**, 1481 (2013).
19. L. Suo, O. Borodin, T. Gao, M. Olguin, J. Ho, X. Fan, C. Luo, C. Wang, and K. Xu, "Water-in-Salt' electrolyte enables high-voltage aqueous lithium-ion chemistries." *Science*, **350**, 938 (2015).
20. R.-S. Kühnel, D. Reber, A. Remhof, R. Figi, D. Bleiner, and C. Battaglia, "'Water-in-Salt' electrolytes enable the use of cost-effective aluminum current collectors for aqueous high-voltage batteries." *Chem. Commun.*, **52**, 10435 (2016).
21. D. Bin, F. Wang, A. G. Tamirat, L. Suo, Y. Wang, C. Wang, and Y. Xia, "Progress in aqueous rechargeable sodium-ion batteries." *Adv. Energy Mater.*, **8**, 1703008 (2018).
22. N. Agmon, "The grotthuss mechanism." *Chem. Phys. Lett.*, **244**, 456 (1995).
23. M. Pourbaix, *Atlas of electrochemical equilibria in aqueous solution* (National Association of Corrosion Engineers (NACE) , Houston, TX) (1974).
24. M. Moskovits and K. H. Michaelian, "A reinvestigation of the Raman spectrum of water." *J. Chem. Phys.*, **69**, 2306 (1978).
25. R. Li, Z. Jiang, F. Chen, H. Yang, and Y. Guan, "Hydrogen bonded structure of water and aqueous solutions of sodium halides: a raman spectroscopic study." *J. Mol. Struct.*, **707**, 83 (2004).
26. K. Furić, I. Ciglenečki, and B. Ćosović, "Raman spectroscopic study of sodium chloride water solutions." *J. Mol. Struct.*, **550–551**, 225 (2000).
27. Q. Sun, "Raman spectroscopic study of the effects of dissolved nacl on water structure." *Vib. Spectrosc.*, **62**, 110 (2012).
28. B. M. Auer and J. L. Skinner, "Ir and Raman spectra of liquid water: theory and interpretation." *J. Chem. Phys.*, **128**, 224511 (2008).
29. N. Dubouis, A. Serva, E. Salager, M. Deschamps, M. Salanne, and A. Grimaud, "The fate of water at the electrochemical interfaces: electrochemical behavior of free water versus coordinating water." *The Journal of Physical Chemistry Letters*, **9**, 6683 (2018).
30. W. Sides, E. Hassani, T.-S. Oh, D. P. Pappas, Y. Hu, and Q. Huang, "Grain growth and superconductivity of rhenium electrodeposited from Water-in-Salt electrolytes." *Journal of Applied Physics*, **127**, 085301 (2020).
31. J. A. Rard, "Chemistry and thermodynamics of ruthenium and some of its inorganic compounds and aqueous species." *Chem. Rev.*, **85**, 1 (1985).
32. M. Guglielmi, P. Colombo, V. Rigato, G. Battaglin, A. Boscolo-Boscoletto, and A. DeBattisti, "'Compositional and microstructural characterization of Ruo2—Tio2 catalysts synthesized by the sol-gel method." *J. Electrochem. Soc.*, **139**, 1655 (1992).
33. N. N. Greenwood and A. Earnshaw, "Iron, Ruthenium and Osmium ." *Chemistry of the Elements* (Elsevier , Amsterdam) 2nd ed. (2012).
34. J. R. Rumble (ed.), "Electrical resistivity of pure metals." *Crc Handbook of Chemistry and Physics* (CRC Press, Boca Raton, FL) 100th ed. (2019).